Performance Enhanced Predictive Control for Adaptive Cruise Control System Considering Road Elevation Information

Shengbo Eben Li, *Senior Member, IEEE*, Qiangqiang Guo, Shaobing Xu, Jingliang Duan, Shen Li, Chengjun Li, and Kuifeng Su

***Abstract*—For road transportation, adaptive cruise control (ACC) is a widely used driver assistance technique with partially longitudinal automation. The existing ACC systems usually ignore the road elevation information, which often ends up with large tracking error and poor fuel economy on the roads with up and down slopes. This paper presents a model-based predictive controller (MPC) for fuel-saving ACC to improve the performances on tracking accuracy and fuel consumption by simultaneously considering the road elevation information, nonlinear powertrain dynamics, and spatiotemporal constraint from preceding vehicle. The feasibility of MPC is enhanced by softening nonsafety related hard constraints, and its asymptotical stability is proved by considering the monotonicity property of a properly chosen Lyapunov function. To efficiently compute the optimal control sequence, a pseudospectral discretization technique, instead of evenly spaced discretization, is adopted to transform the continuous-time optimal control problem into a nonlinear programming. Simulation results demonstrate that the proposed method could reduce fuel consumption by 2.65% in a typical driving scenario and significantly improve the tracking accuracy compared to the one without road slope consideration.**

***Index Terms*—Autonomous vehicle, adaptive cruise control, fuel economy, model predictive control.**

I. Introduction

TO ENHANCE traffic efficiency, improve driving safety, and reduce fuel consumption, various advanced vehicle control systems have been developed to control the vehicle dynamics, e.g., anti-skid traction/braking, electronic stability program (ESP), and longitudinal automation such as cruise control (CC) and adaptive cruise control (ACC) [1]. The CC and ACC systems effectively liberate the driver's throttle and brake operations, thus reducing the driving load. Although some predictive CC systems could acquire look-ahead road information to adjust the vehicle's speed, the existing ACC systems are usually designed for driving on flat highways, and the actual road slope is often ignored or treated as a random disturbance [2]. In real traffic systems, the highways are always accompanied by up and down slopes, which greatly affect the driving load, as well as the engine transmission and bake operations. The absence of slope information will lead to considerable model mismatch and thus result in poor tracking performance [3]. Nowadays the vehicles are capable to acquire road slope data from the precise digital map and/or wireless communication. These technologies provide opportunities to further improve the tracking accuracy of ACC [4]. Furthermore, the prior-known road topology also poses challenges and opportunities to improve the fuel economy, which is often ignored or not concerned by the conventional ACC design [5] [6].

The fuel economy of road vehicles is not only related to the efficiency of vehicle powertrain (e.g., engine and transmission), but also affected by how to control the vehicle, which is commonly referred to the economical driving technologies. The eco-driving applications were estimated to have 10–20% fuel-saving potential in natural traffic systems [7]. The existing researches and projects related to eco-driving are focused on topics including: (i) change driver's behaviors by education or online advices; (ii) fulfill more efficient vehicle automation by directly regulating actuators. The driver education is usually conducted with empirical tips such as driving at economic speed, accelerating less-aggressively, shifting gears sooner to keep engine speed at the economical range, and maintaining steady speed [8]. The projects from European countries showed that such measure is effective in short term with 5–20% fuel savings [8] [9]. While in long term the fuel-saving rate gradually degrades due to the human complacency and behavioral regression [10]. As the ultimate solution, the longitudinal automation systems such as ACC will be the best carriers to perform eco-driving.

In the literature of automatic fuel-saving control, four typical strategies are explored: (1) shorten inter-vehicle distance [11]; (2) cooperative control of engine and powertrain [12]; (3) smoothen longitudinal acceleration [13], [14]; (4) optimize

Manuscript received December 10, 2016; revised June 6, 2017; accepted July 20, 2017. Date of publication August 4, 2017; date of current version October 31, 2017. This work was supported in part by the NSF China under Grant 51575293, Grant 51622504, and Grant U1664263, and in part by the National Key R&D Program in China with Grant 2016YFB0100906. *(Shengbo Eben Li and Qiangqiang Guo contributed equally to this work.) (Corresponding author: Shaobing Xu.)*

S. E. Li, Q. Guo, and J. Duan are with the State Key Laboratory of Automotive Safety and Energy, Department of Automotive Engineering, Tsinghua University, Beijing 100084, China (e-mail: lisb04@gmail.com; gqq14@mails.tsinghua.edu.cn; djl15@mails.tsinghua.edu.cn).

S. Xu is with the Department of Mechanical Engineering, University of Michigan, Ann Arbor, MI 48109 USA (e-mail: xushao@umich.edu).

S. Li is with the Department of Civil and Environmental Engineering, University of Wisconsin-Madison, Madison, WI 53706 USA (e-mail: sli299@wisc.edu).

C. Li and K. Su are with the Autonomous Driving Laboratory, Tencent, Beijing 100084, China (e-mail: chengjunli@tencent.com; kuifengsu@tencent.com).

Color versions of one or more of the figures in this paper are available online at http://ieeexplore.ieee.org.

Digital Object Identifier 10.1109/TIV.2017.2736246

vehicle speed to adapt to road terrain [15]. The first strategy can be effective due to the lower aerodynamic drag when the inter-vehicle distance is shortened, but it usually results in a high risks of rear-end collision. The second strategy regulates engine and transmission simultaneously and aims to increase the probability that engines work in the economic region. Its application, however, is significantly limited by high coordinating complexity of powertrain dynamics. The third strategy reduces the acceleration level to decrease the extra loss of energy produced by aggressive driving. It is quite effective in highly dynamic traffic flow, but less efficient in smooth scenarios. Moreover, it may weaken the tracking capability and introduce frequent cut-ins and cut-offs from adjacent lanes due to large inter-vehicle distance. The fourth strategy, which has been exclusively used in some CC systems, uses the information of upcoming road elevation to adjust desired cruising speed, which enables engine to operation in a more economic manner.

This paper focuses on implementing the fourth strategy on ACC systems. Note that this strategy has been studied in free CC systems, in which the lead vehicle is not considered. For example, Erik *et al.* (2006) designed a dynamic programming-based cruise control scheme with considering road topology to optimize the velocity trajectory and achieved 2.5% fuel-saving benefit [15]. Kamal *et al.* (2011) used the generalized minimal residual method to design an ecological predictive controller with road gradient, which saved 5% fuel [16]. There are two features that distinguish the work in this paper from the above prior studies. First, the aforementioned studies usually simplified engine fueling model as an empirical polynomial of engine power, vehicle speed or longitudinal acceleration. For instance, the fuel mass flow is assumed to be proportional to engine speed in [15], and is estimated by the acceleration and speed in [16]. These simplifications are less accurate to describe the highly nonlinear engine fueling characteristics. In this study, a tabular function of engine torque and engine speed is used to describe the engine fuel, and also a nonlinear dynamics model rather than a linear kinematic model is adopted to describe system behaviors. Second, the CC system does not consider the surrounding vehicles, and longer forward acquisition of road elevation makes the optimal solutions at each step closer to global optimality, thus leading to a better fuel improvement. Different from CC, ACC has to handle the spatiotemporal constraints from surrounding traffic flow, in particular the preceding vehicle, which adds time-varying constraints to the system. In addition, longer prediction horizon results in more inaccurate prediction of the behaviors of preceding vehicle due to the randomness of human behavior when driving.

Generally, model-based predictive control (MPC) is the most widely used method for fuel-saving vehicle automation due to its exceptional capability in implementing optimal control while explicitly handling nonlinearities and constraints [17]. In the literature, MPC has been used in the design of many traditional ACC systems. For instance, Corona & Schutter (2008) used the piece-wise affine model to describe car-following system, and a hybrid MPC is utilized to minimize tracking errors [18]. Li *et al.* (2011) presented a hierarchical MPC controller, in which a quadratic cost function and linear constraints are used to balance multiple objectives such as tracking capability, fuel economy and driver desired response [14]. As far as the authors know, none of them has taken road elevation information into consideration when designing MPC. The lack of road topography may lead to significant tracking error on fluctuating slopes and do harm to fuel economy due to the model mismatch and unpredictable engine operations. This feature could distinguish the proposed control algorithms from the prior designed ACC. Besides, the abovementioned studies usually use a short prediction horizon to decrease computing burden, but a fuel-saving ACC should prolong its prediction horizon to increase the possibility of approximating global optimization, which poses additional challenges on computing efficiency.

The contribution of this paper is to propose a performance enhanced predictive controller for fuel-saving ACC system by simultaneously considering the road elevation, nonlinear powertrain dynamics, and spatiotemporal constraint from preceding vehicle. The pseudospectral technique with unevenly spaced collocation points is adopted to discretize the continuous-time open-loop optimal control (OCP) problem into nonlinear programming (NLP) for numerical computation. The feasibility of MPC is enhanced by softening non-safety related hard constraints, and its asymptotical stability is proved by considering the monotonicity property of a cost function-based Lyapunov function. The direct consideration of road elevation information can avoid the unpredictable engine operations and thus reduce tracking error and fuel consumption.

The rest of this paper is organized as follows: Section II presents the powertrain and engine fuel models. Section III formulates the fuel-saving ACC into an open-loop OCP. Section IV studies the feasibility and stability of MPC. Section V numerically solves the MPC problem. Illustrative examples are given in Section VI. Section VII concludes this paper.

II. Model for Vehicle Longitudinal Dynamics

This paper considers a passenger car equipped with an ACC system, and it has a 2-liter internal combustion engine (ICE) and a continuously variable transmission (CVT). For the sake of controller design, assume that: (1) there is no longitudinal tire slip to four wheels; (2) the engine dynamics are described as a first-order inertial transfer function; (3) for the best fuel economy, the speed ratio of CVT is regulated to always well match the vehicle speed and engine rotating speed; and (4) the nonlinearities and dynamics within driveline are neglected, including flywheel, shaft torsion and gear backslash [19]. The simplified vehicle longitudinal dynamic model is

$$\begin{aligned} M\dot{v} &= \frac{i_g i_0 \eta_T}{r_w} T_e - \frac{T_b}{r_w} - C_A v^2 - Mgf \\ \tau_{eng}\dot{T}_e &= -T_e + T_{ecom} \\ w_e &= \frac{i_g i_0}{r_w} v \end{aligned} \tag{1}$$

where v is the vehicle speed, T_e is the engine torque, T_b is the brake torque, w_e is the engine speed, τ_{eng} is the time constant for engine dynamics, T_{ecom} is the engine torque command, i_g

is the CVT gear ratio, i_0 is the gear ratio of final drive, η_T is the mechanical efficiency of the driveline, r_w is the wheel radius, M is the vehicle mass, C_A is the aerodynamic drag coefficient, g is the gravity coefficient, and f is the coefficient of rolling resistance.

An accurate model of engine fuel consumption is important for fuel-saving vehicle control. The engine fueling characteristics are mainly dominated by the throttle angle and engine speed, and somewhat corrected according to air temperature, intake manifold pressure, tailgate oxygen percentage, etc. Therefore, engine fuel map actually shows an irregular nonlinear property. For the energy management of hybridized powertrains, it is common to use static fuel maps to predict fuel consumption. For internal combustion engine, transient behaviors reduce engine torque by about 4∼5 percent because of incomplete air–fuel mixture and chamber combustion [19]. For fuel-oriented control, it is necessary to consider both static and transient engine fuel. Here, the static fuel is described by the tabular dataset from engine test bed, and fitted as a two-dimensional polynomial function. The fitted polynomial of engine brake specific fuel consumption (BSFC) map is

$$b_s\left(T_e, w_e\right) = \sum_{i=0}^{N} \sum_{j=0}^{i} \psi_{i,j} \left(T_e\right)^{i-j} \left(w_e\right)^{j} \tag{2}$$

where $b_s(\cdot,\cdot)$ is engine BSFC, $\psi_{i,j}$ is the fitting coefficient of N-th order polynomials. Here, N is selected to be 4 to balance complexity and accuracy. The transient fuel consumption is designed as a correction term related to the torque varying rate, and integrated into the static map-based fuel model:

$$F_d\left(T_e, w_e\right) = b_s\left(T_e, w_e\right) P_e + k_e \left(\frac{\mathrm{d}T_e}{\mathrm{d}t}\right)^2 \tag{3}$$

where $F_d(\cdot,\cdot)$ is the engine fuel rate, including both static and transient fuel, k_e is the coefficient for transient fuel. In addition, the maximum engine torque $T_{\max}$ is described as a fourth order polynomial of engine speed:

$$T_{\max} = \sum_{i=0}^{4} k_{ci} {w_e}^i \tag{4}$$

where k_{ci} is the fitting coefficient. To achieve the best engine efficiency, the CVT is controlled to follow the optimal BSFC line, as shown in Fig. 1, which gives the lowest fuel consumption under a specific fixed engine power. The optimal BSFC line is fitted as

$$T_e = k_{eco}(w_e - w_{\text{emin}})^{\gamma} \tag{5}$$

where k_{eco} is the fitting coefficient, $w_{e\min}$ is the minimum engine speed, γ is the exponent.

III. Optimal Control Problem in Predictive Horizon

The basic function of an ACC system is to track the motion of a preceding vehicle by regulating the engine torque and/or braking torque command. In a car-following scenario, the two consecutive vehicles run on hilly road, as shown in Fig. 2.

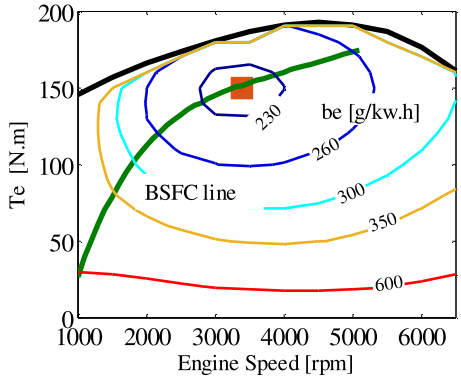

Fig. 1. The engine BSFC map.

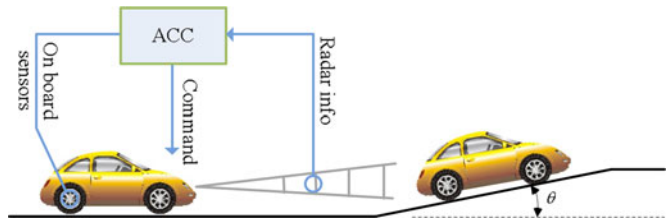

Fig. 2. Cruise control concept of road vehicle.

For the sake of controller design, assume that: (1) the preceding and following vehicles run on a straight road without curve, or the curve is big enough to overlook the lateral dynamics of the vehicles. (2) the speed and position of preceding vehicle could be real-timely accessed by the following vehicle. By employing constant time-headway (CTH) policy, such a car-following system is mathematically modeled by

$$\begin{aligned} \dot{\Delta} d &= \Delta v - \tau_h a_p \\ \dot{\Delta} v &= a_f - \left(\frac{i_g i_0 \eta_T}{M r_w} T_e - \frac{T_b}{r_w} - \frac{C_A}{M} v^2 - gf\right) + g\theta \\ \dot{T}_e &= -\frac{1}{\tau_{eng}} T_e + \frac{1}{\tau_{eng}} T_{ecom} \end{aligned} \tag{6}$$

where Δd is the distance error, which is defined as $\Delta d = d - d_h$, $d_h = \tau_h v_p + d_0$. d is the relative distance between preceding and following vehicle, v_p is the speed of preceding vehicle, τ_h is the time headway, d_0 is the constant safety distance. Δv is the relative speed defined as $\Delta v = v_p - v_f$. a_p is the acceleration of preceding vehicle, and θ is the road slope,. Note that the road slope θ is prior-known by technologies such as GIS and GPS.

The design of fuel-saving ACC naturally casts into a model predictive control framework, in which engine fuel consumption is minimized as a cost function, while other requirements can be enforced as equality and/or inequality constraints. Here, we take engine fuel consumption directly as the cost function, and a balance with the tracking error is also considered (noted as

Problem A1):

$$J_{ACC} = \int_0^T \left\{ \lambda \cdot \left(\left(\frac{\Delta d}{SDE\,(v)} \right)^2 + \left(\frac{\Delta v}{SRV\,(v)} \right)^2 \right) + (1-\lambda) \cdot F_d\,(T_e, w_e) \right\} dt, \tag{7}$$

where J_{ACC} is the performance index of ACC, T is the predictive horizon, $SDE(v)$ is a function of vehicle speed, called sensitivity to distance error, and $SRV(v)$ is also a function of vehicle speed, called sensitivity to relative speed, $\lambda \in [0,1]$ is the weighting coefficient to balance tracking errors and fuel economy. Note that the predicted speed of preceding vehicle in $[0,T]$ is calculated as the sum of current speed and the product of current acceleration and time t. As suggested by Li *et al.* [6], the sensitivity function actually described the driver expected control gain for tracking errors, expressed as:

$$\begin{aligned} SDE(v)^{-1} &= k_{SDE} v + d_{SDE} \\ SRV(v)^{-1} &= k_{SRV} v + d_{SRV} \end{aligned} \tag{8}$$

where k_{SDE}, d_{SDE} are fitting coefficients for driver expected SDE, and k_{SRV}, d_{SRV} are fitting coefficients for driver expected SRV. In naturalistic driving, drivers use different control gain for tracking errors at different speed. In general, the control gains become smaller with increasing speed, which implies that driver tends to lose the accurate control of tracking errors when speed goes up (accompanying with larger inter-vehicle distance). This phenomenon is particularly true for the condition when drivers regulate the distance error [6]. The ACC system should also satisfy the following equality and inequality constraints:

a) Physical constraints

$$\begin{aligned} w_{\text{emin}} \le w_{\text{e}} \le w_{\text{emax}} \\ T_{\text{min}} < T \le T_{\text{max}} \\ i_{\text{gmin}} \le i_{\text{g}} \le i_{\text{gmax}} \end{aligned} \tag{9}$$

b) Tracking error constraints

$$\begin{aligned} \frac{\Delta d_{\text{min}}}{SDE\,(v)} \le \Delta d \le \frac{\Delta d_{\text{max}}}{SDE\,(v)} \\ \frac{\Delta v_{\text{min}}}{SRV\,(v)} \le \Delta v \le \frac{\Delta v_{\text{max}}}{SRV\,(v)} \end{aligned} \tag{10}$$

c) Comfort constraint

$$a_{\text{min}} \le \dot{v} \le a_{\text{max}} \tag{11}$$

d) Speed limit constraints

$$v \le v_{\text{limit}} \tag{12}$$

e) Rear end safety constraints

$$d > d_{safe}, d_{safe} = \min\{d_0, TTC \cdot \Delta v\} \tag{13}$$

where *TTC* is the allowed minimum time-to-collision.

The constraint (a) is from physical limit of engine and transmission, not allowed to be violated. The constraint (b) is from the driver desired bounds of tracking errors. Too large inter-vehicle distance might induce frequent cut-ins from adjacent lanes, and too small inter-vehicle distance might increase the risk of rear-end collision. The driver desired bounds are statistically summarized by driver experiment data. In addition, the bounds are corrected by using SDE and SRV function to adapt vehicle speed. The constraint (c) is from the requirement of driver ride comfort because large acceleration and deceleration is objectionable to human comfort. The constraint (d) is the road speed limit, in case that the leading vehicle validates infrastructure rules enforced by traffic management sector. The constraint (e) is the rear-end safety constraint. The minimum inter-vehicle distance is set to be larger than zero, and any rear-end collision is never expected.

IV. Feasibility and Stability Analysis of MPC

In the abovementioned problem, the constraints (9)∼(13) are hard constraints because their bounds were not allowed to be violated. Pursuing better fuel economy often leads to smooth accelerating/decelerating process. The tracking errors sometimes unavoidably reach their bounds due to the weaken accelerating/decelerating capability. In such cases, the straightforward result of receding horizon optimization is to strengthen engine torque in accelerating scenarios or strengthen braking force in decelerating scenarios. This approach, however, is not always realistic because the vehicle acceleration is mostly located on its bounds in some extreme situations, leaving no space to be strengthened further. Therefore, the infeasibility naturally emerges because the tracking errors keep increasing or decreasing along their previous directions. The constraint softening method is an effective way to address infeasibility in receding horizon optimization. The essential idea is to penalize constraint violations instead of imposing hard constraints, thus allowing the solution of MPC whenever the hard constraints are infeasible [20]. Here, we will use this approach to soften some hard constraints to eliminate infeasibility.

Another, but more important, topic is the issue of closed-loop stability of MPC system. MPC cannot guarantee the closed-loop stability for finite-horizon cost functions, especially for short prediction horizon [21]. Additional ingredients are needed in the cost function and/or constraints to ensure stability, which somehow re-formulates original MPC problems. Using additional conditions to ensure the stability of linear MPC is often easier than the nonlinear cases. Commonly used approaches include complementing the cost function with a zero-state terminal constraint [22], adding a terminal penalty which equals to the infinite-horizon cost [23], etc. Although there is well-established theory for linear cases, its importance diminishes because MPC with nonlinearities and constraints is hardly better than infinite horizon linear quadratic (LQ) control. For nonlinear cases, it has been proved in [24] that the zero-state terminal constraint guarantees closed-loop stability, although it might cause some additional computation burden. An improvement of zero-state constraint is called dual-mode method, which replaces the equality constraints by inequalities for the terminal states [25]. In the dual-mode control, the MPC switches to a stable linear control, e.g., LQ, once the terminal states in the prediction horizon enter a suitable neighborhood of the equilibrium points. This method reduces the possibility of infeasibility at the expense of frequent

switching on the bounds of the neighborhood. Another stabilizing method is to use the terminal contractive constraints, which require that the norm of the terminal states is sufficiently smaller than that of the initial states in the prediction horizon [26]. Key mechanisms to guarantee stability fall into three ingredients: (1) using terminal equality or inequality constraint; (2) incorporating the penalty of final state into cost function, (3) using both terminal cost and terminal constraint.

Considering both the issues of feasibility and stability, we modify the cost function into (14), and Constraint (b), (c) into soft constraints (noted as **Problem A2**):

$$J = J_{ACC} + \phi\left(\Delta d\left(T\right), \Delta v\left(T\right)\right) + \rho\varepsilon^2, \tag{14}$$

f) Tracking error constraints

$$\begin{aligned} \Delta d_{\min} - \varepsilon\zeta_d \le \Delta d \le \Delta d_{\max} + \varepsilon\zeta_d \\ \Delta v_{\min} - \varepsilon\zeta_v \le \Delta v \le \Delta v_{\max} + \varepsilon\zeta_v \end{aligned} \tag{15}$$

g) Comfort constraint

$$a_{f\min} - \varepsilon\zeta_a \le a_f \le a_{f\max} + \varepsilon\zeta_a$$

where $\varepsilon \ge 0$ is the slack variable, $\phi(\cdot,\cdot)$ is the Mayer function for terminal state, and $\zeta_\#$ are the relaxing coefficients for different variables. Note that constraints (d) and (e) are not soften because of lawsuit reasons for driving safety. Once their bounds are reached, a solution is to issue warnings and then hand over control authority to drivers. Besides, for the Mayer function $\phi(\cdot,\cdot)$, a matched terminal constraint (h) is added to guarantee the closed loop stability:

h) Terminal inequality constraint

$$\begin{aligned} \left|\Delta d\left(T\right)\right| &\le \Delta d_f \\ \left|\Delta v\left(T\right)\right| &\le \Delta v_f \\ \left|T_e\left(T\right)\right| &\le T_{ef} \end{aligned} \tag{16}$$

where Δd_f, Δv_f and T_{ef} are the bounds of terminal inequality constraints. Note that (16) can be equality constraint only if $\Delta d_f = 0, \Delta v_f = 0$ and $T_{ef} = 0$. The problem is solved numerically to obtain the optimal control trajectory $u^0(t), t \in [0, T]$, and the value of $u^*(0)$ at $t = 0$ is used for the current time step control. It should be noted that because of time invariance, both Problem (A1) and (A2) assumed that the current time is $t = 0$.

For narrative convenience in stability proof, Problem (A2) is rewritten to be generic form as follows (noted as **Problem A3**)

$$\begin{aligned} J\left(t, x, u, \varepsilon, T\right) = \phi\left(x\left(T\right)\right) + \int_t^{t+T} l\left(x\left(\tau\right), u\left(\tau\right)\right) d\tau \\ + \rho\varepsilon(t)^2 \end{aligned} \tag{17}$$

Subject to

$$\dot{x(t)} = f\left(x\left(t\right), u\left(t\right)\right) \tag{18}$$

with both hard and soft constraints

$$\begin{aligned} u &\in \mathbb{U} + \zeta_u \varepsilon\left(t\right) \\ x &\in \mathbb{X} + \zeta_x \varepsilon\left(t\right) \\ \varepsilon\left(t\right) &\ge 0 \end{aligned} \tag{19}$$

and terminal constraint

$$x\left(t+T\right) \le X_f \tag{20}$$

where t is the current time, T is the predictive horizon, $f : (\mathbb{R}^n, \mathbb{R}^m) \to \mathbb{R}^n$ is the function of plant model. There exists a dual pair $(\bar{x}, \bar{u}) \in (\mathbb{X},\ \mathbb{U}) \in (\mathbb{R}^n, \mathbb{R}^m)$ which satisfies $f(\bar{x}, \bar{u}) = 0$. The sets $\mathbb{X} \in \mathbb{R}^n$ and $\mathbb{U} \in \mathbb{R}^m$ are hard constraints for the state and input, and $\zeta_u,\ \zeta_x$ are related to corresponding soft constraints. The function $l : (\mathbb{R}^n, \mathbb{R}^m) \to \mathbb{R}$ is the non-negative definite function of (x, u), i.e.,

$$l\left(x, u\right) > 0, \forall\ f\left(x, u\right) \ne 0,\ u \in \mathbb{U}, x \in \mathbb{X} \tag{21}$$

and $\phi :\ \mathbb{R}^n \to \mathbb{R}$ is the functio of $x(T)$, and $X_f \in \mathbb{X} \in \mathbb{R}^n$ describes the terminal constraint on final state. The main theorem for stability is stated as follows:

Theorem: Problem (A3) is asymptotically stable if satisfying:

(B1) $X_f \in \mathbb{X}$, closed;
(B2) $\kappa_f(x) \in \mathbb{U}, \forall x \in X_f$;
(B3) X_f is positively invariant for $\dot{x} = f(x(t), \kappa_f(x))$;
(B4) $\dot{\phi}(x) + l(x, \kappa_f(x)) \le 0, \forall x \in X_f$,

where $\kappa_f(x)$ is a local controller for $t = T$.

Proof: Define a Lyapunov function

$$V^0\left(t, T\right) = \min_{u,\varepsilon}\left\{J\left(t, x, u, \varepsilon, T\right)\right\} \tag{22}$$

As suggested in [21], [22], [23] and therein, it is assumed that $V^0(t, T)$ is continuously differentiable. Then the fake Hamilton-Jacobi-Bellman equation always holds for Problem (A3) (Magni & Sepulchre, 1997 [27])

$$l\left(x, u\right) + \frac{\partial V^0\left(t, T\right)}{\partial T} + \frac{\partial V^0\left(t, T\right)}{\partial x} f\left(x, \kappa^0\left(x\right)\right) = 0 \tag{23}$$

where $\kappa^0(x)$ represents optimal control for u. The key point is to prove so-called monotonicity property, i.e.,

$$\frac{\partial V^0\left(t, T\right)}{\partial T} \ge 0 \tag{24}$$

Recall the fact used in [27]:

$$\frac{\partial V^0\left(t, T\right)}{\partial T} = \lim_{\tau \to 0} \frac{V^0\left(t, T+\tau\right) - V^0\left(t, T\right)}{\tau} \tag{25}$$

The symbol $u^0(t), \varepsilon^0(t)$ represent the optimal control strategy for time horizon $[t, t+T]$. Let define a new control for time horizon $[t, t+T+\tau]$

$$\begin{aligned} \tilde{u}\left(t\right) &= \begin{cases} u^0\left(t\right), & [t, t+T] \\ \kappa_f\left(x\left(T\right)\right), & (t+T, t+T+\tau] \end{cases} \\ \tilde{\varepsilon}\left(t\right) &= \varepsilon^0\left(t\right), \ [t, t+T+\tau] \end{aligned} \tag{26}$$

Note that $\kappa_f(x(T))$ should be feasible local controller, satisfying (B2) and (B3). The corresponding state with respect to $\tilde{u}, \tilde{\varepsilon}$ is denoted as $\tilde{x}$. Then, we have

$$\begin{aligned} V^0(t, T+\tau) &= J\left(t, x^0, u^0, \varepsilon^0, T+\tau\right) \\ &\le J(t, \tilde{x}, \tilde{u}, \tilde{\varepsilon}, T+\tau) \\ &= \phi(x(t+T+\tau)) \\ &\quad + \int_t^{t+T+\tau} l(x,u)\, d\tau + \rho\tilde{\varepsilon}(t)^2 \\ &= V^0(t,T) + \int_{t+T}^{t+T+\tau} l(x,u)\, d\tau \\ &\quad + \phi(x(t+T+\tau)) \\ &\quad - \phi(x(t+T)) \end{aligned} \tag{27}$$

In (27), the first line comes from optimality condition. Then, rescheduling (27) into (28):

$$\begin{aligned} & V^0(t, T+\tau) - V^0(t,T) \\ & \le \int_{t+T}^{t+T+\tau} l(x,u)\, d\tau \\ & \quad + \phi(x(t+T+\tau)) \\ & \quad - \phi(x(t+T)) \end{aligned} \tag{28}$$

Divided (28) by τ and we have when $\tau \to 0$:

$$\frac{\partial V^0(t,T)}{\partial T} \le l(x(T), \kappa_f(x(T))) + \dot{\phi}(x(t+T)) \le 0 \tag{29}$$

Then by (23), it is concluded that

$$\dot{V}^0(t,T) = \frac{\partial V^0(t,T)}{\partial x} f\left(x, \kappa^0(x)\right) < 0 \tag{30}$$

■

In this paper, the terminal constraint of (20) is set as 0, which means that (B1) and (B3) are satisfied. Besides, $l(x, \kappa_f(x)) = 0$ is always satisfied under such terminal constraint. There is no Mayer function $\phi(\cdot,\cdot)$ in the proposed optimal control problem, so (B4) is satisfied. $\kappa_f(x) \in \mathbb{U}$ is a free control input to be optimized, thus (B2) is satisfied. In all, Problem (A3) is asymptotically stable.

V. Transformation Using Pseudospectral Discretization

A. Basis of Pseudospectral Discretization

The plant dynamics are described by time-continuous first order differential equations. For numerical computation, the continuous problem should be converted into time-discrete description for the computer environment [28]. The typical approach for this conversion is to discretize the plant model, constraints, and cost function at evenly spaced points. The evenly spaced discretization approach is widely used in the literature, e.g., Chen & Allgower, 1998 [29]. In this approach, the system behaviors between two consecutive collocation points are usually approximated by either zero order hold (ZOH) or first order hold (FOH), which are the two lowest order approximation methods [30]. This feature leads to relatively high state prediction error and integral error. Hence, more sampling points are needed to achieve sufficient accuracy, which however result in high computational load.

The pseudospectral method is an efficient approach to achieve high computing accuracy with much less collocation points for nonlinear constrained system. It was first applied to optimal control problems in the late 1980's [31]. The pseudospectral methods are often categorized into three types: Lobatto, Gauss, and Radau pseudospectral. The first type uses the family of Lobatto quadrature. The collocation points are the Legendre-Gauss-Lobatto (LGL) points. The second and third methods use the family of Gauss and Radau quadrature, respectively [32]. In this study, we adopt the first method for the efficient implementation of the proposed MPC.

To convert the OCP into an associated nonlinear programming problem (NLP), it discretizes the OCP at orthogonal collocation points and then uses global interpolating polynomials to approximate the states and control inputs [33]. The state space equations are represented as equality constraints. The integral of cost function is calculated by the Gauss-Lobatto quadrature rule. Then, the OCP is converted into a NLP problem, which can be solved by mature optimization solvers, like SNOPT used here. The detailed framework is described below.

Step 1: Time-domain transformation

For simplicity, we first transform the time domain $[0, T]$ to the canonical interval $[-1, 1]$:

$$\tau = (2t - T)/(T),\ \tau \in [-1, 1] \tag{31}$$

Step 2: Collocation and discretization

For pseudospectral methods, the collocation points often come from the roots of orthogonal polynomials, which also help avoid the Runge phenomenon. Let $P_N(\tau)$ denote the Legendre polynomial of order N. The orthogonal collocation points are the Legendre-Gauss-Lobatto (LGL) points, which include two parts: (1) $\tau_i,\ \ i = 1,\ 2, \ldots,\ N-1$, being the zeros of $\dot{P}_N(\tau)$, i.e., the derivative of $L_N(\tau)$; and (2) $\tau_0 = -1$ and $\tau_N = 1$. The state variable $\boldsymbol{x}(\tau)$ and control variable $\boldsymbol{u}(\tau)$ are discretized at points $\{\tau_0, \tau_1, \ldots, \tau_N\}$. The discretized state vectors are denoted by $\{\boldsymbol{X}_0, \boldsymbol{X}_1, \ldots, \boldsymbol{X}_N\}$ and the discretized control vectors are denoted by $\{\boldsymbol{U}_0, \boldsymbol{U}_1, \ldots, \boldsymbol{U}_N\}$, where $\boldsymbol{X}_i = \boldsymbol{x}(\tau_i)$ and $\boldsymbol{U}_i = \boldsymbol{u}(\tau_i)$. Then we approximate $\boldsymbol{x}(\tau)$ and $\boldsymbol{u}(\tau)$ by

$$\begin{aligned} \boldsymbol{x}(\tau) &\approx \boldsymbol{X}(\tau) = \sum_{i=0}^{N} L_i(\tau)\, \boldsymbol{X}_i, \\ \boldsymbol{u}(\tau) &\approx \boldsymbol{U}(\tau) = \sum_{i=0}^{N} L_i(\tau)\, \boldsymbol{U}_i, \end{aligned} \tag{32}$$

where $L_i(\tau)$ is called the Lagrange basis function:

$$L_i(\tau) = \prod_{\mathrm{j}=0,\mathrm{j}\neq\mathrm{i}}^{\mathrm{N}} (\tau - \tau_j)/(\tau_i - \tau_j) \tag{33}$$

Step 3: Conversion of the state space equations

The differential state equations can be approximated by the differential operation on the Lagrange basis polynomials. Namely the derivatives of state vector could be approximated by a differentiation matrix multiplied with discretized state variables, i.e.,

$$\dot{\boldsymbol{x}}\left(\tau_k\right) \approx \dot{\boldsymbol{X}}_{\boldsymbol{k}} = \sum_{i=0}^{N} \dot{L}_i\left(\tau_k\right) \boldsymbol{X}_i = \sum_{i=0}^{N} D_{ki} \cdot \boldsymbol{X}_i \tag{34}$$

where $k = 0,\ 1, \ldots,\ N$, $\boldsymbol{D} = (D_{ki})$ is an $(N+1) \times (N+1)$ differentiation matrix described as follows:

$$D_{kj} = \begin{cases} \frac{P_N(\tau_k)}{P_N(\tau_i)(\tau_k - \tau_i)}, & i \neq k \\ -\frac{N(N+1)}{4}, & i = k = 0 \\ \frac{N(N+1)}{4}, & i = k = N \\ 0, & \text{otherwise} \end{cases} \tag{35}$$

The state space equations can be transformed to the equality constraint at the LGL collocation points:

$$\sum_{i=0}^{N} D_{ki} \cdot \boldsymbol{X}_i - \frac{T}{2} f\left(\boldsymbol{X}_k, \boldsymbol{U}_k\right) = 0 \tag{36}$$

Step 4: Conversion of the cost function

The integral part of the cost function is calculated by Gaussian-Lobatto quadrature, so the performance index is computed by

$$J\left(t, x, u, \varepsilon, T\right) = \phi\left(X_N\right) + \frac{T}{2} \sum_{i=0}^{N} w_i l\left(X_i, U_i\right) + \rho\varepsilon(t)^2 \tag{37}$$

where w_i is the weight coefficient of the Gauss-Lobatto quadrature rule, defined as

$$w_i = \int_{-1}^{1} L_i\left(\tau\right) d\tau = \frac{2}{N\left(N+1\right) P_N^2\left(\tau_I\right)} \tag{38}$$

Step 5: Convert the OCP problem to the NLP problem

The OCP of the MPC can be converted to a NLP problem using the aforementioned pseudospectral method.

$$\min J = \phi\left(X_N\right) + \frac{T}{2} \sum_{i=0}^{N} w_i l\left(X_i, U_i\right) + \rho\varepsilon(t)^2$$

Subject to

$$\begin{aligned} &\sum_{i=0}^{N} D_{ki} \cdot \boldsymbol{X}_i - \frac{T}{2} f\left(\boldsymbol{X}_k, \boldsymbol{U}_k\right) = 0, \\ &k = 0, \ldots, n-1; \quad i = 0, \ldots, N-1. \\ &\boldsymbol{X}_N - \boldsymbol{X}_f \leq 0, \\ &\boldsymbol{X}_i \in \mathbb{X} \in \mathbb{R}^n, \\ &\boldsymbol{U}_i \in \mathbb{U} \in \mathbb{R}^m. \end{aligned} \tag{39}$$

This NLP is a high-dimensional sparse constrained problem, and is solved by the Sequential Quadratic Programming (SQP) algorithm with SNOPT [34].

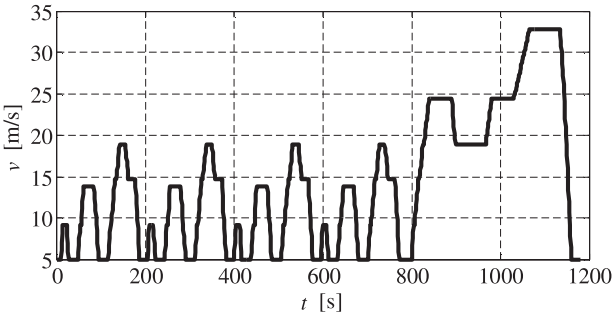

Fig. 3. Preceding vehicle's speed from a modified NEDC.

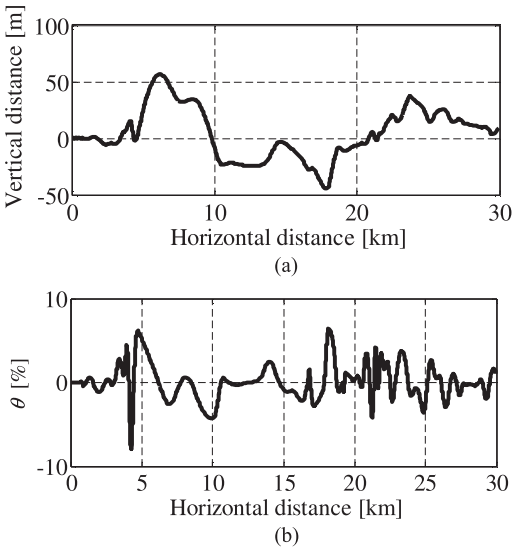

Fig. 4. Road structure and slope. (a) Road elevation. (b) Road slope.

VI. Simulations and Analyses

Tracking and fuel saving performances of the proposed ACC is assessed by simulations in this section. The preceding vehicle runs along the speed profile modified from the New European Driving Cycle (NEDC). The NEDC is designed to contain long-term idling for testing the emission level and fuel economy. To avoid the idling, an extra 5 m/s is added to the original NEDC speed. The maximal speed is inhibited to 33 m/s considering the speed limit of highway. The preceding vehicle's speed for simulation is shown in Fig. 3. Since there is no standard road slope profiles to test controllers, a sinusoidal road topography is adopted for simulation, as shown in Fig. 4. The main parameters of vehicle model are listed in Table I. The number of collocation points of pseudospectral method is set to 10. The initial distance gap between the two vehicles is set to 11.5 m with a constant time-headway of 1.5 s.

A. Influence of Prediction Horizon

The normal MPC-based ACC usually adopts relatively short prediction time (e.g., 1 second) to reduce the computation burden in numerical optimization. But the fuel-saving ACC should prolong the prediction horizon to broaden optimization space and to achieve better fuel economy. However, as the prediction

TABLE I
PARAMETERS OF THE VEHICLE MODEL

Parameter	Value	Parameter	Value
M	1600 kg	$\omega_{\min}$	1000 rpm
η_T	0.90	$\omega_{\max}$	6000 rpm
C_A	0.43 kg/m	$T_{\min}$	0 Nm
f	0.027	$T_{\max}$	180 Nm
r_w	0.307 m	τ_{eng}	0.35 s
k_e	1×10^{-3}	i_0	3.863
k_{SDE}	0.106 s/m	d_{SDE}	0.678
k_{SRV}	−0.002 s/m	d_{SRV}	1.025

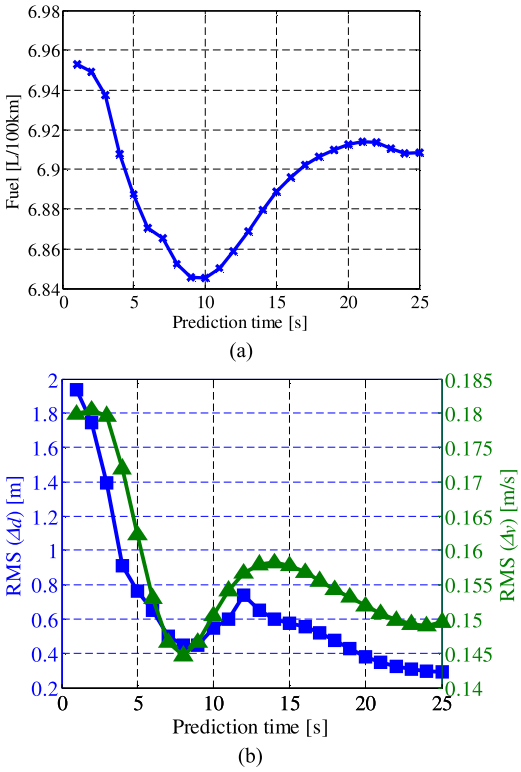

Fig. 5. Performance under different prediction horizon. (a) Fuel consumption. (b) RMS of range error and speed error.

horizon becomes longer, the prediction of preceding vehicle's behavior tends to be less accurate, which conversely makes the fuel optimization worse. To balance these factors, the proposed MPC controller is tested under different prediction horizon and the results are shown in Fig. 5.

The root mean squares of range error ($RMS(\Delta d)$) and speed error ($RMS(\Delta v)$) are used to evaluate the performance of tracking ability. Fig. 5(a) shows that the fuel consumption decreases 1.7% when the prediction time increases from 1 s to 10 s. As the prediction time keeps growing, the fuel consumption increases again, because an overlong horizon leads to less accurate prediction of the lead vehicle. The range error and speed error reduce remarkably when the prediction horizon increases from 1 s to 8 s, and then decrease slowly as the prediction time keeps increasing. These results imply that a prediction horizon of 8 s is enough to achieve near-optimal tracking accuracy, but is not the best balance when considering fuel economy. The reasonable

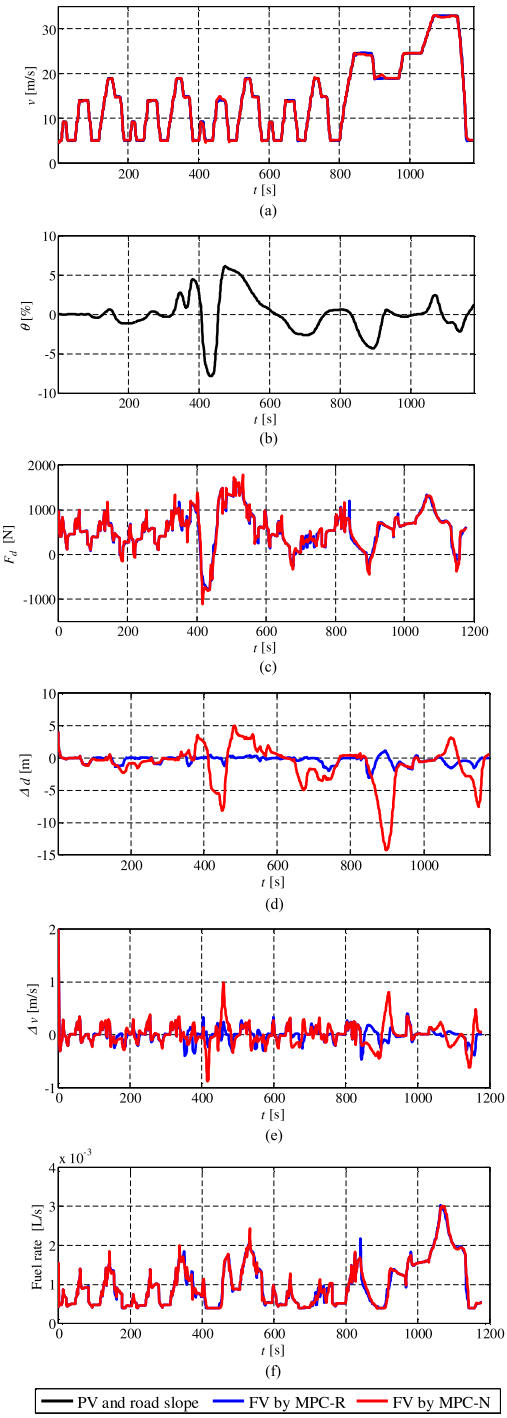

Fig. 6. Performance of different controllers. (a) Speed. (b) Road slope. (c) Driving force. (d) Range error. (e) Speed error. (f) Fuel rate.

balance falls into the range of 8 s to 12 s. This paper will select 10 s as the prediction time for the following simulations.

B. Comparison Between MPC w/ and w/o Road Topography

Both the MPC-based ACC controllers with and without road slope information are simulated, indicated by MPC-R and MPC-N, respectively. Fig. 6(a) shows the speed profiles of the preceding vehicle (PV) and the following vehicle (FV) of MPC-N

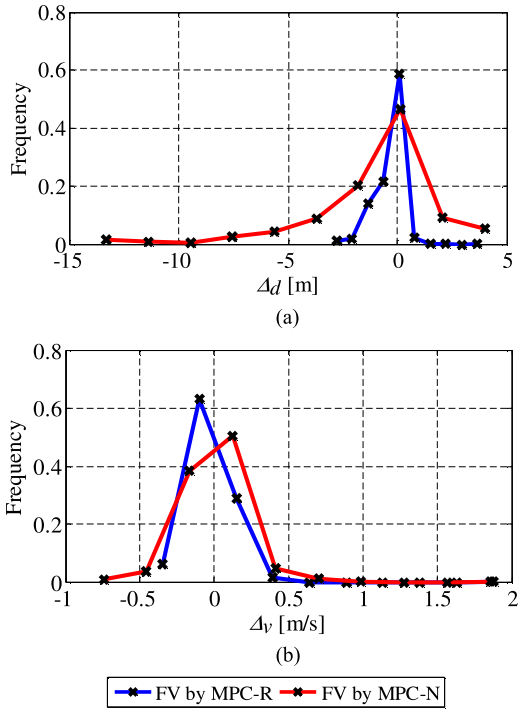

Fig. 7. Tracking error distribution of the two controllers. (a) Range error. (b) Speed error.

TABLE II
ECONOMY PERFORMANCE

	MPC-N	MPC-R	Improve
Fuel consumption (L/100 km)	7.0076	6.8496	2.25%
average range error (Absolute value)	1.95 m	0.47 m	75.90%
average speed error (Absolute value)	0.14 m/s	0.10 m/s	28.57%

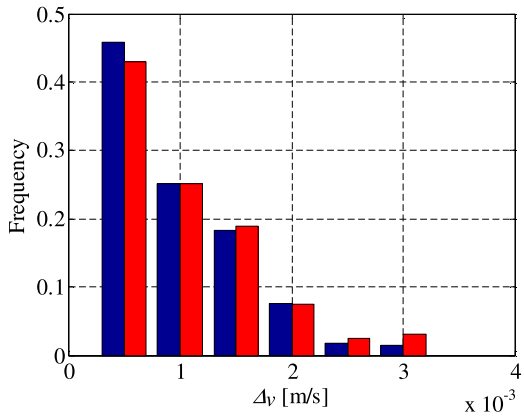

Fig. 8. Frequency distribution of fuel rate.

and MPC-R. Fig. 6(b) shows the road slope. The driving force including the drive and brake is shown in Fig. 6(c). The tacking error of distance and speed are shown in Fig. 6(d) and (e) respectively, and fuel rate is given in Fig. 6(f).

It is observed that MPC-R achieved better tracking performance than MPC-N. For example, when the road slope changes to negative values, the total resistance decreases, which then causes over high acceleration. The surfeit of acceleration reduces the range between the FV and PV, then the controller adopts lower engine torque and even brake operation to maintain a safe tracking distance. For MPC-N, with no road topography information, the engine torque and brake force cannot be precisely controlled thus a severe negative range error is generated. As the range error becomes higher, the controller increases the brake force to reduce the error, which is shown in Fig. 6(c). For MPC-R, the adjustment process is quite similar to MPC-N except that the prior awareness of road slope enables the controller to control the engine torque and brake force more accurately, thus the tracking errors are suppressed. Fig. 6(d) and (e) demonstrates that the range and speed error of MPC-R are much smaller and are adjusted more quickly than MPC-N. The root mean squares of range error of MPC-R is 76.63% lower compared to MPC-N. The root mean squares of speed error is also reduced by 27.99%.

To further evaluate the tracking performance, the distributions of range error and speed error of the two controllers are shown in Fig. 7, and the absolute average errors are list in Table II. Fig. 7(a) shows that the range of tracking error starts from -15 m and stops at $+5$ m when controlled by MPC-N. While the error of MPC-R is limited in the range of $[-3, 4]$ m, and the average error is about 75.90% lower than that of MPC-N. Fig. 7(b) shows the speed error of the two controllers. The average speed error of MPC-R is roughly 28.57% lower than that of MPC-N

Fig. 6(f) shows the engine fueling rate of the two controllers. The engine operations of MPC-R have relatively smaller fluctuation. In the statistical view, the frequency graph of the fuel rate is shown in Fig. 8. It is shown that the fuel rate of MPC-R is lower than MPC-N except for the lowest level. The fuel consumptions of these two controllers over the whole modified NEDC are listed in Table II. The results indicate that MPC-R improves the fuel economy by 2.25% compared to MPC-N in this simulation case.

VII. CONCLUSION

This paper presented a performance enhanced predictive controller for adaptive cruise control system considering the road elevation information, nonlinear powertrain dynamics, and spatiotemporal constraint from preceding vehicle. The road slope information is integrated into the controller directly to optimize the vehicle motion for better tracking accuracy and fuel economy. The feasibility of this controller is enhanced by softening non-safety related hard constraints, and its asymptotical stability is proved by considering the monotonicity property of a properly-chosen Lyapunov function. The simulation results show that compared to a normal controller, the average tracking distance error is reduced about 76% and the average speed error drops about 29%. Apart from the improvement on tracking ability, it also reduces fuel consumption by 2.25% in the given sinusoidal slope scenario.

REFERENCES

[1] K. Bengler, K. Dietmayer, B. Farber, M. Maurer, C. Stiller, and H. Winner, "Three decades of driver assistance systems: Review and future perspectives," *IEEE Intell. Transp. Syst. Mag.*, vol. 6, no. 4, pp. 6–22, 2014.

[2] C. Liang and H. Peng, "Optimal adaptive cruise control with guaranteed string stability," *Veh. Syst. Dyn.*, vol. 32, no. 4/5, pp. 313–330, 1999.

[3] S. Xu, S. E. Li, B. Cheng, and K. Li, "Instantaneous feedback control for a fuel-prioritized vehicle cruising system on highways with a varying slope," *IEEE Trans. Intelli. Transp. Sys.*, vol. 18, no. 5, pp. 1210–1220, May 2017.

[4] K. Lidström *et al.*, "A modular CACC system integration and design," *IEEE Trans. Intell. Transp. Sys.*, vol. 13, no. 3, pp. 1050–1061, Sep. 2012.

[5] G. Bifulco, L. Pariota, F. Simonelli, and R. Di Pace, "Development and testing of a fully adaptive cruise control system," *Transp. Res. Part C, Emerg. Technol.*, vol. 29, pp. 156–170, 2013.

[6] S. E. Li, K. Li, and J. Wang, "Economy-oriented vehicle adaptive cruise control with coordinating multiple objectives function," *Veh. Syst. Dyn.*, vol. 51, no. 1, pp. 1–17, 2013.

[7] A. Atabani, I. Badruddin, S. Mekhilef, and A. Silitonga, "A review on global fuel economy standards, labels and technologies in the transportation sector," *Renew. Sustain. Energy Rev.*, vol. 15, no. 9, pp. 4586–4610, 2011.

[8] B. Beusen, "Using on-board logging devices to study the longer-term impact of an eco-driving course," *Transp. Res. Part D*, vol. 14, pp. 514–520, 2009.

[9] J. Barkenbus, "Eco-driving: An overlooked climate change initiative," *Energy Policy*, vol. 38, pp. 762–769, 2010.

[10] M. Zarkadoula, G. Zoidis, and E. Tritopoulou, "Training urban bus drivers to promote smart driving: A note on a Greek eco-driving pilot program," *Transp. Res. Part D, Transp. Environ.*, vol. 12, no. 6, pp. 449–451, 2007.

[11] M. Hammache, M. Michaelian, and F. Browand, "Aerodynamic forces on truck models, including two trucks in tandem," SAE, Warrendale, PA, USA, Tech. Paper 2002-01-0530, 2002.

[12] J. Ino, T. Ishizu, and H. Sudou, "Adaptive cruise control system using CVT gear ratio control," *SAE Trans.*, vol. 110, no. 7, pp. 675–680, 2001.

[13] A. Bose and P. Ioannou, "Analysis of traffic flow with mixed manual and semi-automated vehicles," *IEEE Trans. Intell. Transp. Sys.*, vol. 4, no. 4, pp. 173–188, Dec. 2003.

[14] S. Li, K. Li, R. Rajamani, and J. Wang, "Model predictive multi-objective vehicular adaptive cruise control," *IEEE Trans. Control Sys. Tech.*, vol. 19, no. 3, pp. 556–566, May 2011.

[15] E. Hellström, A. Fröberg, and L. Nielsen, "A real-time fuel-optimal cruise controller for heavy trucks using road topography information," SAE, Warrendale, PA, USA, Tech. Paper 2006-01-0008, 2006.

[16] M. Kamal, M. Mukai, J. Murata, and T. Kawabe, "Model predictive control of vehicles on urban roads for improved fuel economy," *IEEE Trans. Control Sys. Tech.*, vol. 21, no. 3, pp. 831–841, May 2013.

[17] L. Bageshwar, L. Garrard, and R. Rajamani, "Model predictive control of transitional maneuvers for adaptive cruise control vehicles," *IEEE Trans. Veh. Tech.*, vol. 53, no. 5, pp. 1573–1585, Sep. 2004.

[18] D. Corona and D. Schutter, "Adaptive cruise control for a SMART car: A comparison benchmark for MPC-PWA control methods," *IEEE Trans. Control Sys. Tech.*, vol. 16, no. 2, pp. 365–372, Mar. 2008.

[19] S. E. Li and H. Peng, "Optimal strategies to minimize fuel consumption of passenger cars during car-following scenarios," *J. Automob. Eng.*, vol. 226, no. 3, pp. 419–429, 2012.

[20] A. Gautam and Y. Soh, "Constraint softening in model predictive control with off-line-optimized admissible sets for systems with additive and multiplicative disturbances," *Syst. Control Lett.*, vol. 69, pp. 65–72, 2014.

[21] D. Mayne, J. Rawlings, C. Rao, and P. Scokaert, "Constrained model predictive control: Stability and optimality," *Automatica*, vol. 36, no. 6, pp. 789–814, 2000.

[22] W. Kwon and A. Pearson, "On feedback stabilization of time-varying discrete-linear system," *IEEE Trans. Autom. Control*, vol. 23, no. 3, pp. 479–481, Jun. 1978.

[23] J. Rawlings and K. Muske, "The stability of constrained receding horizon control," *IEEE Trans. Autom. Control*, vol. 38, no. 10, pp. 1512–1516, Oct. 1993.

[24] S. Keerthi and E. Gilbert, "Optimal infinite-horizon feedback laws for a general class of constrained discrete-time systems: Stability and moving-horizon approximations," *J. Optim. Theory Appl.*, vol. 57, no. 2, pp. 265–293, 1988.

[25] T. Yang and E. Polak, "Moving horizon control of nonlinear systems with input saturation, disturbances and plant uncertainty," *Int. J. Control*, vol. 58, no. 4, pp. 875–903, 1993.

[26] D. Mayne, J. Rawlings, C. Rao, and P. Scokaert, "Constrained model predictive control: Stability and optimality," *Automatica*, vol. 36, no. 6, pp. 789–814, 2000.

[27] L. Magni and R. Sepulchre, "Stability margins of nonlinear receding horizon control via inverse optimality," *Syst. Control Lett.*, vol. 32, pp. 241–245, 1997.

[28] L. Magni and R. Scattolin, "Model predictive control of continuous-time nonlinear systems with piecewise constant control," *IEEE Trans. Autom. Control*, vol. 49, no. 6, pp. 900–906, Jun. 2004.

[29] H. Chen and F. Allgöwer, "A quasi-infinite horizon nonlinear model predictive control scheme with guaranteed stability," *Automatica*, vol. 34, no. 10, pp. 1205–1217, 1998.

[30] D. Dehaan and M. Guay, "A real time framework for model predictive control of continuous time nonlinear systems," *IEEE Trans. Autom. Control*, vol. 52, no. 11, pp. 2047–2056, Nov. 2007.

[31] G. Elnagar and M. Razzaghi, "A collocation-type method for linear quadratic optimal control problems," *Optim. Control Appl. Methods*, vol. 18, no. 3, pp. 227–235, 1998.

[32] I. Ross and M. Karpenko, "A review of pseudospectral optimal control: From theory to flight," *Annu. Rev. Control*, vol. 36, no. 2, pp. 182–197, 2012.

[33] S. Xu, S. E. Li, K. Deng, S. Li, and B. Cheng, "A unified pseudospectral computational framework for optimal control of road vehicles," *IEEE/ASME Trans. Mechatronics*, vol. 20, no. 4, pp. 1499–1510, Aug. 2015.

[34] P. Gill, W. Murray, and M. Saunders, "SNOPT: An SQP algorithm for large-scale constrained optimization," *SIAM Rev.*, vol. 47, no. 1, pp. 99–131, 2005.

Shengbo Eben Li (M'13–SM'16) received the M.S. and Ph.D. degrees from Tsinghua University, Beijing, China, in 2006 and 2009, respectively. He worked at Stanford University, University of Michigan, and University of California Berkeley. He is currently the Associate Professor in the Department of Automotive Engineering, Tsinghua University. He is the author of more than 100 peer-reviewed journal/conference papers, and the co-inventor of more than 20 Chinese patents. His active research interests include intelligent and connected vehicles, learning-based driver assistance, distributed control and optimal estimation, electrified powertrain management, etc. Dr. Li serves as the TPC member of IEEE Intelligent Vehicle Symposium, ISC member of FAST-zero 2017 in Japan, and Associated editor of IEEE INTELLIGENT TRANSPORTATION SYSTEMS MAGAZINE and IEEE TRANSACTIONS ON INTELLIGENT TRANSPORTATION SYSTEMS, etc. He received the Best Paper Award in 2014 IEEE Intelligent Transportation System Symposium, the Best Paper Award in 14th ITS Asia Pacific Forum, the National Award for Technological Invention in China (2013), the Excellent Young Scholar of NSF China (2016), the Young Professorship of Changjiang Scholar Program (2016).

Qiangqiang Guo received the B.S. degree from the Department of Automotive Engineering, Tsinghua University, Beijing, China, in 2014. He is currently working toward the M.S. degree. Since 2014, he has been a Research Assistant in the Intelligent Safety and Human Factors Laboratory, Tsinghua University. His research interests include autonomous vehicle control, eco-driving and assistance, and driver behavior analysis.

Shaobing Xu received the B.S. degree in automotive engineering from China Agricultural University, Beijing, China, in 2011, and the Ph.D. degree in mechanical engineering from Tsinghua University, Beijing, China, in 2016. He is currently a Postdoc Research Fellow in the Department of Mechanical Engineering, University of Michigan, Ann Arbor, MI, USA. His research interests include autonomous vehicle, optimal control theory, vehicle control strategy design, and SLAM. He received the outstanding Ph.D. dissertation award of Tsinghua University, the First Prize of the Chinese 4th Mechanical Design Contest, and the First Prize of the 19th Advanced Mathematical Contest.

Jingliang Duan received the B.S. degree from the College of Automotive Engineering, Jilin University, Changchun, China, in 2015. He is currently working toward the Ph.D. degree. Since 2015, he has been a Research Assistant of the Intelligent Safety and Human Factors Laboratory, Tsinghua University, Beijing, China. His research interests include decision making of autonomous vehicle, traffic flow, and driver behavior analysis.

Shen Li received the B.S. degree in automotive engineering from Jilin University, Changchun, China, in 2012. He is currently working toward the Ph.D. degree in the Department of Civil and Environmental Engineering, University of Wisconsin, Madison, WI, USA. His research interests include autonomous vehicle, traffic flow theory, traffic status estimation, and Big Data.

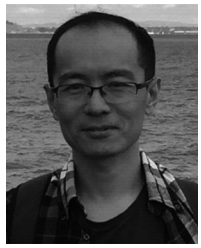

Chengjun Li received the Ph.D. degree in Computer Science from Peking University, Beijing, China, in 2007. He worked at Honeywell for 4 years and joined Tencent in 2011. He is now leading the Autonomous Driving Lab within Tencent Map. His active research interests include computer graphics, street view, HAD map, autonomous vehicle, and robotics.

Kuifeng Su received the Ph.D. degree in Computer Science from Tsinghua University, Beijing, China, in 2013. Before joining Tencent, he worked at The Academy of Armored Forces Engineering. He is now working at the Autonomous Driving Lab within Tencent Map. His active research interests include autonomous vehicles, perception and decision making, vehicle dynamics and control.